Electronic Supplementary Information

Synthesis of Multiarm Star Copolymers Based on Polyglycerol Cores with Polylactide Arms and Their Application as Nanocarriers

M. Adeli,[a, b] H. Namazi[c], F. Du[a], S. Hönzke[d], S. Hedtrich[d], J. Keilitz[a], R. Haag*[a]

[a]*Institute of Chemistry and Biochemistry, Freie Universität Berlin, Takustr. 3, D-14195 Berlin, Germany; Phone: +49-30-838-52633; Fax: +49-30-838-53357; E-mail: haag@chemie.fu-berlin.de. Homepage: http://www.polytree.de.*

[b]*Department of Chemistry, Faculty of Science, Lorestan University, Khoramabad, Iran*

[c]Lab of Dendrimers and Biopolymers, Faculty of Chemistry, University of Tabriz, Tabriz, P. O. Box: 51664, Iran

[d]*Institute of Pharmacy (Pharmacology and Toxicology), Freie Universität Berlin, Berlin, Germany*

Table of Contents:

1. Figure S1. ^{1}HNMR spectra of multi arm star copolymers containing PG_{8000} in $CDCl_3$ solvent…….....pg. 4

2. Figure S2. IR spectra of multi arm star copolymers containing a) PG_{2400} and b) PG_{8000}……....pg.5

3. Calculation of molecular weight of multiarm star copolymers using ^{1} HNMR spectra…….……...pg.6

4. Figure S3. Relation between molecular weight and [LA]/[OH] ratio for multi arm star copolymers containing a) PG_{2400} and b) PG_{8000} cores……..……pg.7

5. Figure S4. GPC diagram of multiarm star copolymers containing PG_{8000} and PG_{2400} cores……...……...…….……pg.8

6. Figure S5. TGA thermograms of multiarm star copolymers containing a) PG_{8000} and b) PG_{2400} series…….……pg. 9

7. Tables S1 and S2. Thermal properties of PG_{8000}-PLA and PG_{2400}-PLA multiarm star copolymers respectively……pg. 10

8. Figure S6. Photograph of encapsulated Congo red by multiarm star copolymer containing PG_{8000} core…….……pg.10
9. Figure S7. UV spectra of chloroform solution of the host-guest systems of multiarm star copolymers containing PG_{8000} core……...…….pg. 11
10. Figure S8. UV spectra of chloroform solution of the host-guest systems of multiarm star copolymers containing PG_{2400} core……...…….pg. 11
11. Figure S9. UV spectra of encapsulated 5-ASA by multiarm star copolymers containing hPG_{2400} core and synthesized by 6.25, 12.5, 25 and 50 [LA]/[OH] ratios in chloroform solution……..pg. 12
12. Figure S10. Arm number versus the [LA]/[OH] ratio for multiarm star copolymers containing PG_{8000} core……pg. 13
13. Figure S11. UV spectra of encapsulated 5-ASA by PG_{8000}-PC_{25} and PG_{2400}-PC_{25} multi arm star copolymers…….....pg.13
14. Figure S12. Size of nanocarriers constructed using different ratio of [LA]/[OH] and PG_{8000} core ……..……...……..pg.14
15. Figure S13. Polydispersity of nanocarriers constructed using different ratio of [LA]/[OH] and PG_{8000} core in chloroform solvent ……pg.14
16. Figure S14. Size of nanocarriers constructed using different ratio of [LA]/[OH] and PG_{2400} core..……...…….……pg.15
17. Figure S15a. TEM of solid nanocarriers obtained by evaporation of chloroform from 0.4 g/L solution of nanocarriers…...……...pg.15
18. Figure S15b. TEM of solid nanocarriers obtained by evaporation of chloroform from 1 g/L solution of nanocarriers ……pg.15
19. Figure S15c and d. TEM of solid nanocarriers obtained by evaporation of chloroform from 0.4 g/L solution of nanocarriers…….pg. 15
20. Figure S16. TEM of solid nanocarriers obtained by evaporation of chloroform from a, b, c and d) 0.4 g/L, e) 1 g/L, f) 5 g/L solution of nanocarriers……Pg. 16
21. Figure S17. TEM images of for hPG_{8000}-PLA_{25}. Scale bar is 50 nm……. Pg. 17
22. Figure S18. Release of guest molecule from chloroform solution of PG_{2400}-PLA nanocarriers to the water phase……..... Pg. 19

23. Figure S19. Release of guest molecule from chloroform solution of PG_{8000}-PLA nanocarriers to the water phase……... Pg. 19
24. Figure S20. Encapsulation of Congo red by PG_{8000}-PLA_{25} nanocarrier…… Pg. 20
Figure S21. Encapsulation of Congo red by PG_{8000}-PLA_{100} nanocarrier……. Pg. 20
25. Figure S22. Release of 5-ASA from host-guest systems containing a) PG_{8000}-PLA and b) PG_{2400}-PLA nanocarriers in pH 1…….. Pg. 22
26. Figure S23. Release of 5-ASA from host-guest systems containing a) PG_{2400}-PLA b) PG_{8000}-PLA in pH 7.4…… Pg. 23
27. Figure S24. Release of 5-ASA from a) PG_{2400}-PLA and b) PG_{8000}-PLA nanocarriers in pH 12…….. Pg. 24
28. Figure S25. DLS diagrams of PG_{8000}-$PLA_{6.25}$ and PG_{8000}-$PLA_{12.5}$ nanocarriers in water at polymer concentration of 0.5 mg/ml……..25
29. Figure S26. DLS diagrams of PG_{8000}-$PLA_{6.25}$ and PG_{8000}-$PLA_{12.5}$ nanocarriers containing Nile red in water at polymer concentration of 0.5 mg/ml……25
30. Figure S27. Zeta-potential diagrams of a) PG_{8000}-$PLA_{6.25}$ and b) PG_{8000}-$PLA_{12.5}$ nanocarriers containing Nile red in water at polymer concentration of 0.5 mg/ml…….26
31. Figure S28. UV spectra of encapsulated Nile red by PG_{8000}-$PLA_{12.5}$ nanocarriers in water with a certain polymer concentration and increased Nile red amount…….27

Figure S1 show the ^{1}HNMR spectra of multiarm star copolymers containing dendritic PG with 8000 (PG_{8000}) molecular weight. Signals of PLA chains appear at 1.25-1.9 ppm and 5-5.3 ppm for protons of methyl and CH groups respectively also chemical shifts of PG are seen at 2.65-2.90 ppm and 3.2-4 ppm for protons of free (unreacted) OH groups and methylene groups respectively. Signals of protons of conjugated methylene of PG to PLA arms and end CH groups of PLA chains are appeared at 4-4.5 ppm as a overlapped signal. As it can be seen in this figure with increasing the [LA]/[OH] ratio intensity of signals of PG is diminished. This result shows a direct relationship between the length and number of PLA chains and monomer ratios. In the high ratios (for example [LA]/[OH]= 100 in this figure) PG signals are disappeared.

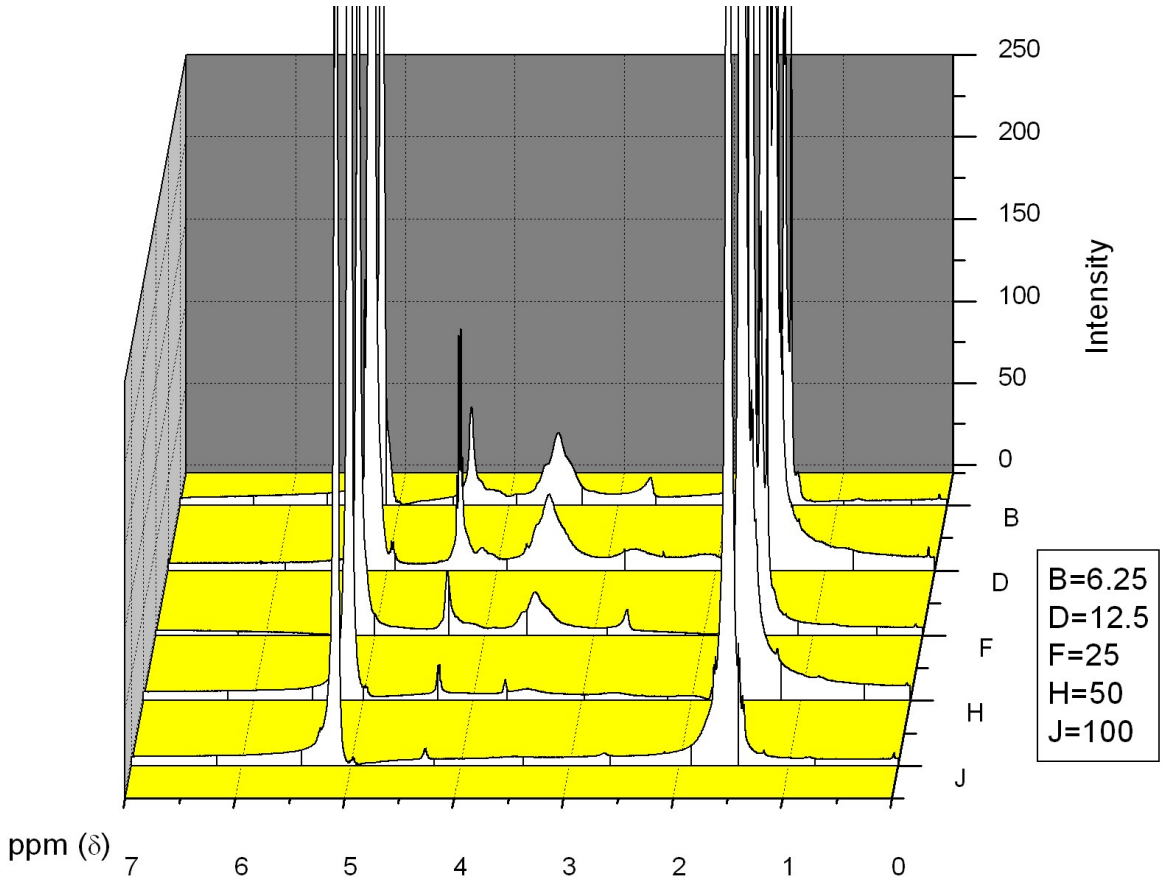

Figure S1. ^{1}HNMR spectra of multi arm star copolymers containing PG_{8000} in $CDCl_3$ solvent

Figure S2 shows the IR spectra of multiarm star copolymers containing PG_{8000} core. In this figure with increasing the [LA]/[OH] ratios the OH absorbance band of PG is decreased and this display the growth of PLA chains on the PG core.

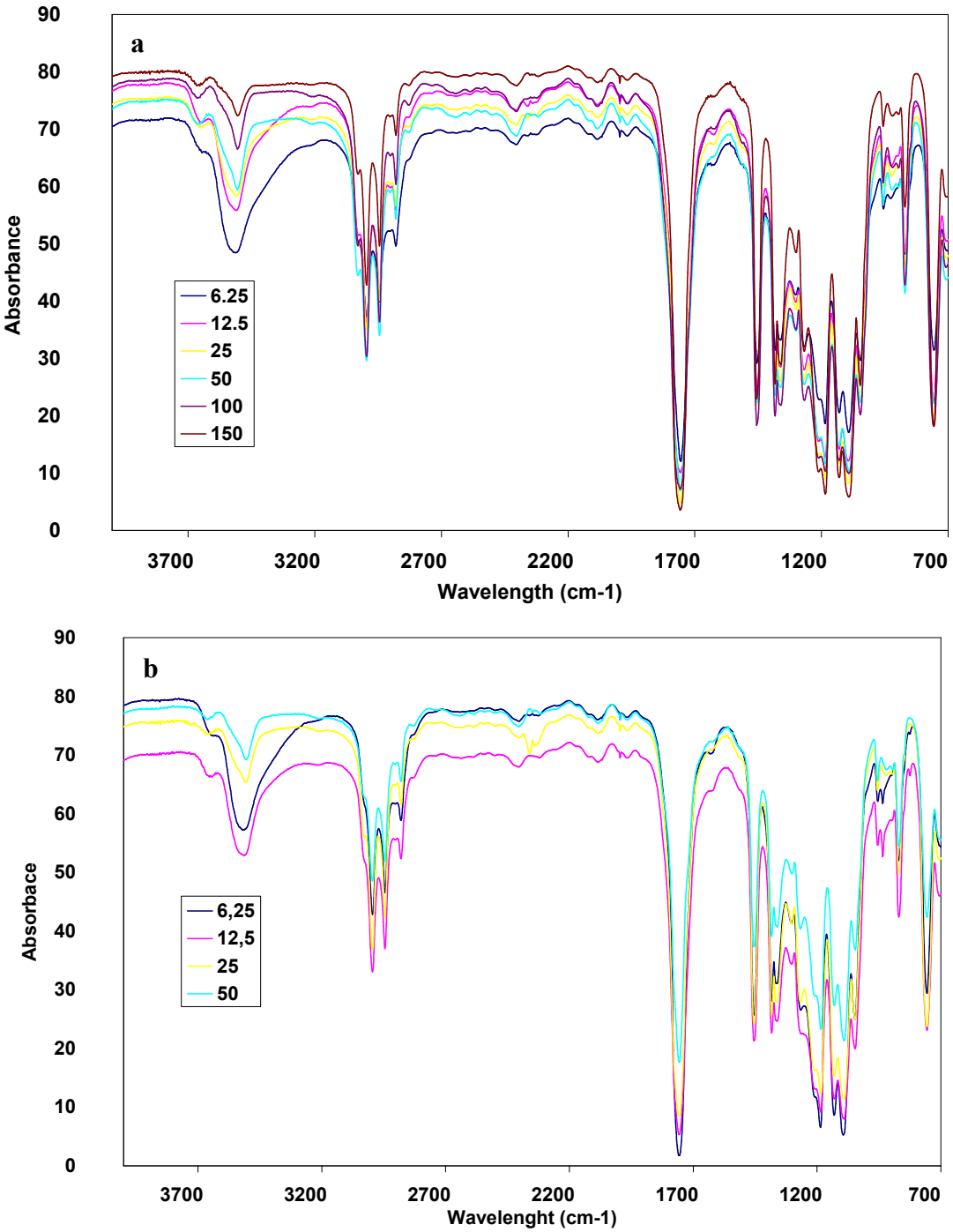

Figure S2. IR spectra of multiarm star copolymers containing a) PG_{2400} and b) PG_{8000} cores

Calculation of the molecular weight of multiarm star copolymers using ^{1} HNMR spectra:

The characteristics of multiarm star copolymers were determined using ^{1}H NMR spectra. Calculations for multiarm star copolymer containing PG_{8000} core and constructed using [LA]/[OH]= 6.25 ratio are shown below:

M = Integral of signal at 4.3 ppm

For obtaining of integral of reacted methylene protons of PG:

M/3= N

N×2=Y

Y= Integral of reacted methylene protons of PG

Because this signal is containing the signal of protons of reacted methylene groups of PG and end CH groups of arms. So for every arm we have two methylene proton and one end CH proton.

0.98/3= 0.32

0.32×2= 0.64

PG with 8000 molecular weight has 530 methylene protons

530-X/X= 2/0.64

X= 130

Every methylene group has two protons

130/2=65 arms

0.32/1= 5.86/M

5.86 = peak area of –CH- groups in the backbone of PLA

M/2= DP =9

Mn= 9×65×144+8000= 92240

Figure S3 display the relation between [LA]/[OH] ratio and molecular weight of multiarm star copolymers containing PG_{2400} and PG_{8000} core. Molecular weight of copolymers is increased with increasing of [LA]/[OH] ratio and it show that control of molecular weight of multiarm star copolymers is possible by [LA]/[OH] ratio.

Increasing the molecular weight of multiarm star copolymers was determined by GPC measurements. Figure S4 show increasing of the molecular weight of multiarm star copolymers containing PG_{2400} core versus [LA]/[OH] ratio.

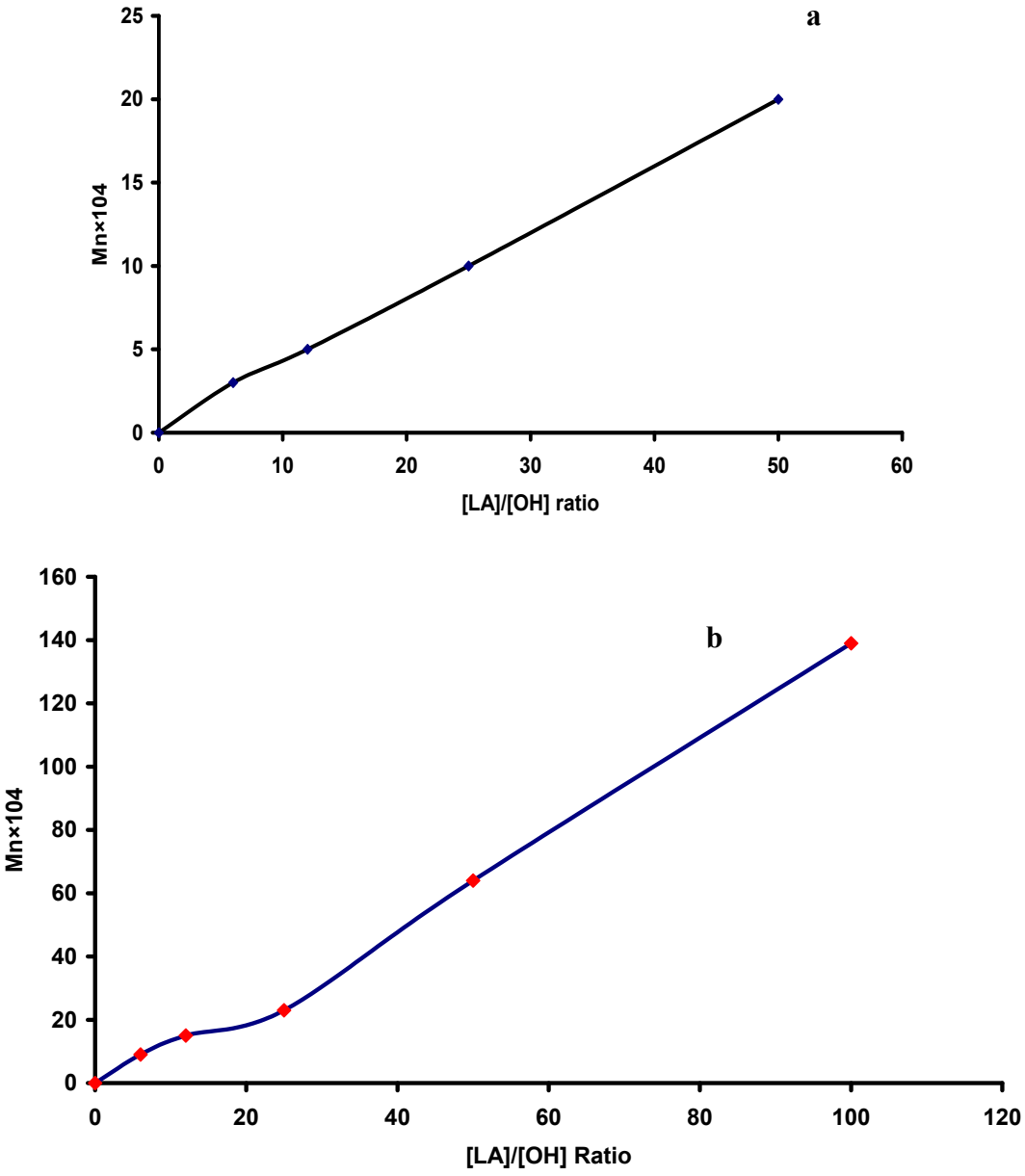

Figure S3. Relation between molecular weight and [LA]/[OH] ratio for multiarm star copolymers containing a) PG_{2400} and b) PG_{8000} cores

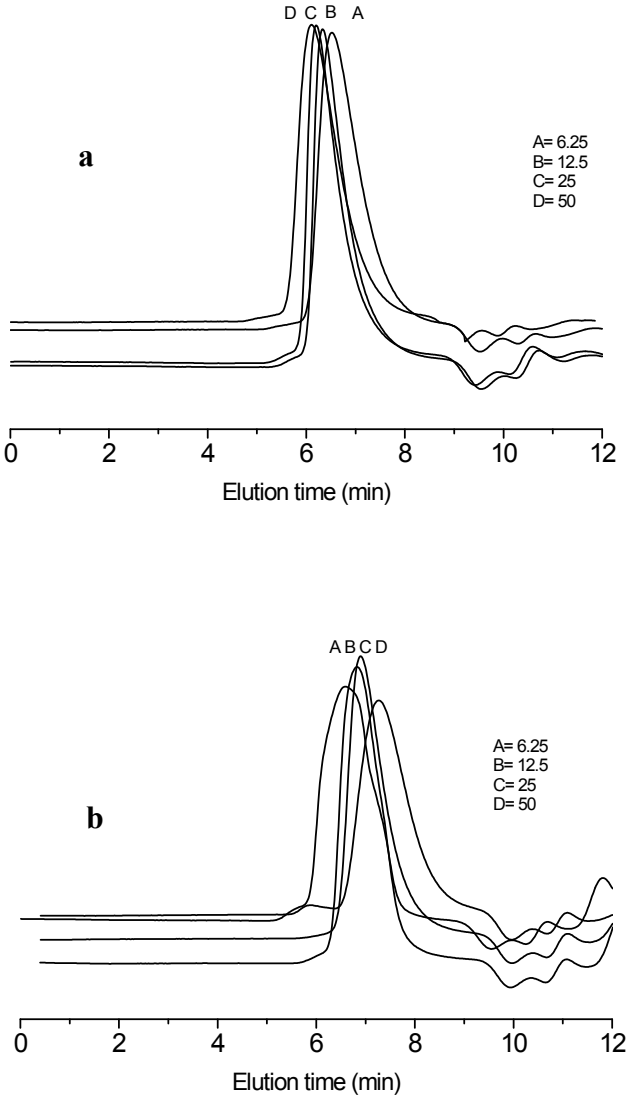

Figure S4. GPC diagram of multiarm star copolymers containing a) PG_{8000} and b) PG_{2400} cores.

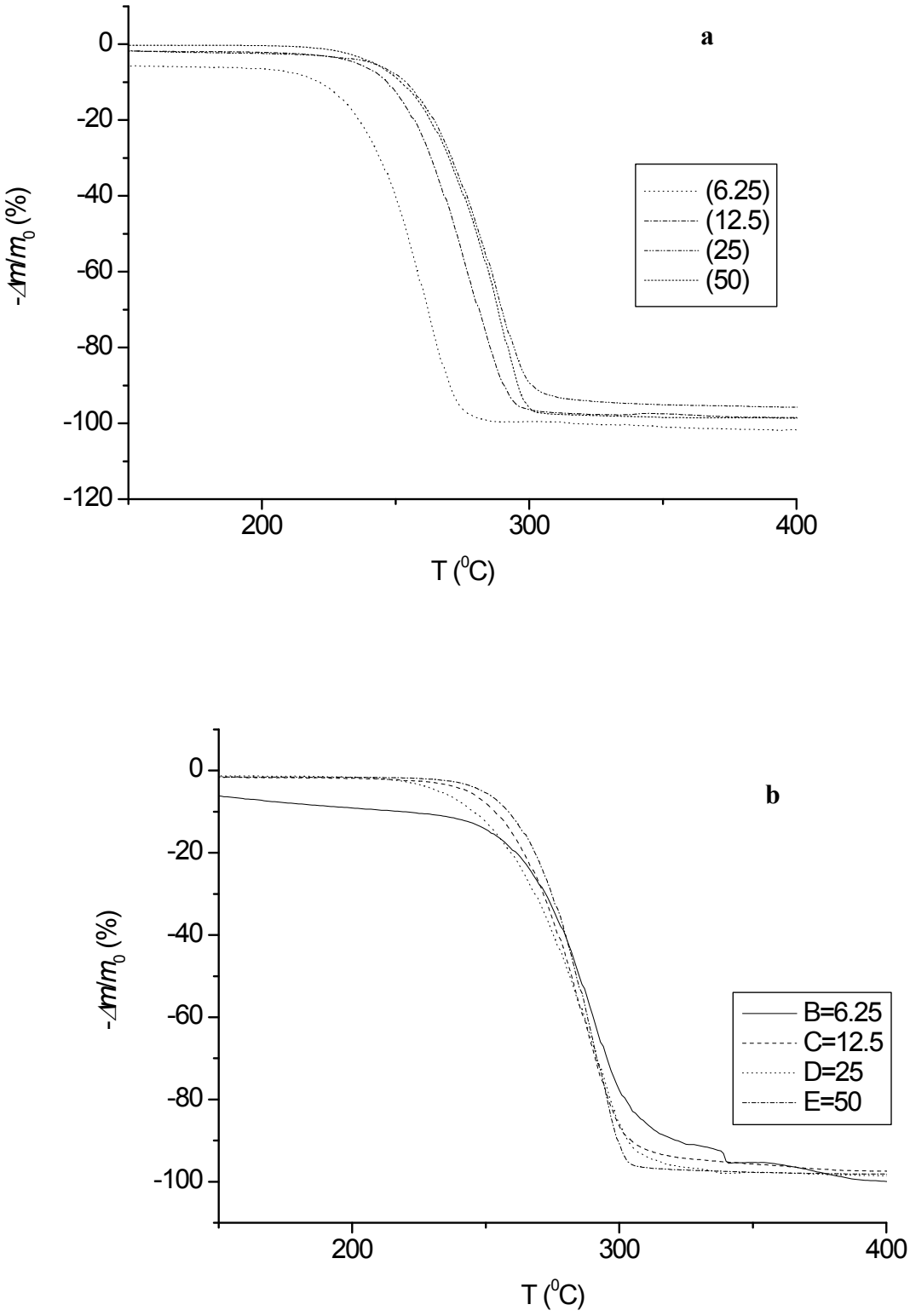

Figure S5. TGA thermograms of multiarm star copolymers containing a) PG_{8000} and b) PG_{2400} series

Sample	[LA/OH]	T 20% [°C]	T 50% [°C]	T(max) [°C]
1	6.25	236	255	271
2	12.5	257	273	291
3	25	264	281	302
4	50	265	281	307

Table S1. Thermal properties of PG_{8000}-PLA multiarm star copolymers

Sample	(LA/OH)	T 20% (ºC)	T 50% (ºC)	T(max) (ºC)
1	6.25	262	258	322
2	12.5	264	282	305
3	25	260	281	303
4	50	269	284	300

Table S2. Thermal properties of PG_{2400}-PLA multiarm star copolymers

Figure S6. shows the photograph of encapsulated Congo red by multiarm star copolymers in chloroform. It can be seen that with increasing the molecular weight (arm number and length of arms) TC of these compounds is increased.

Figure S6. Photograph of encapsulated Congo red by multiarm star copolymer containing PG_{8000} core

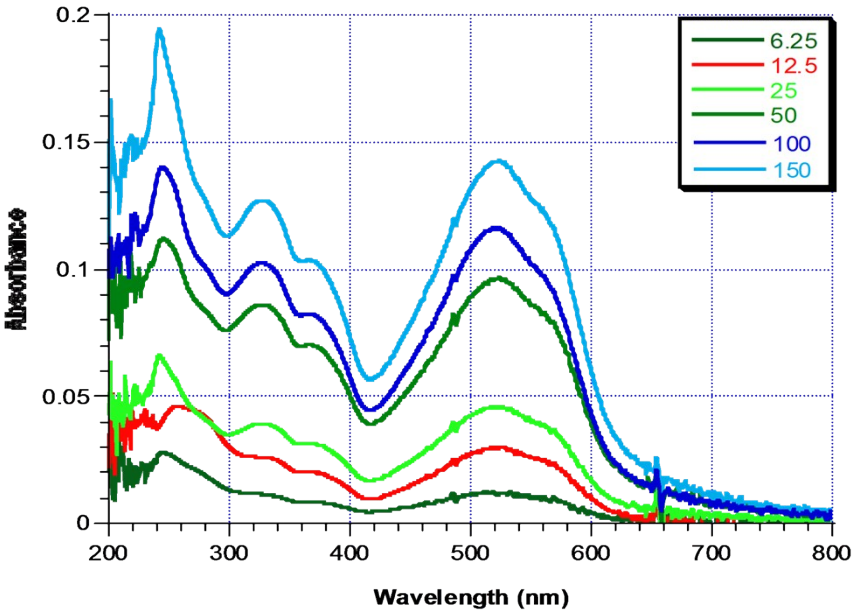

Figure S7. UV spectra of chloroform solution of the host-guest systems of multiarm star copolymers containing PG_{8000} core

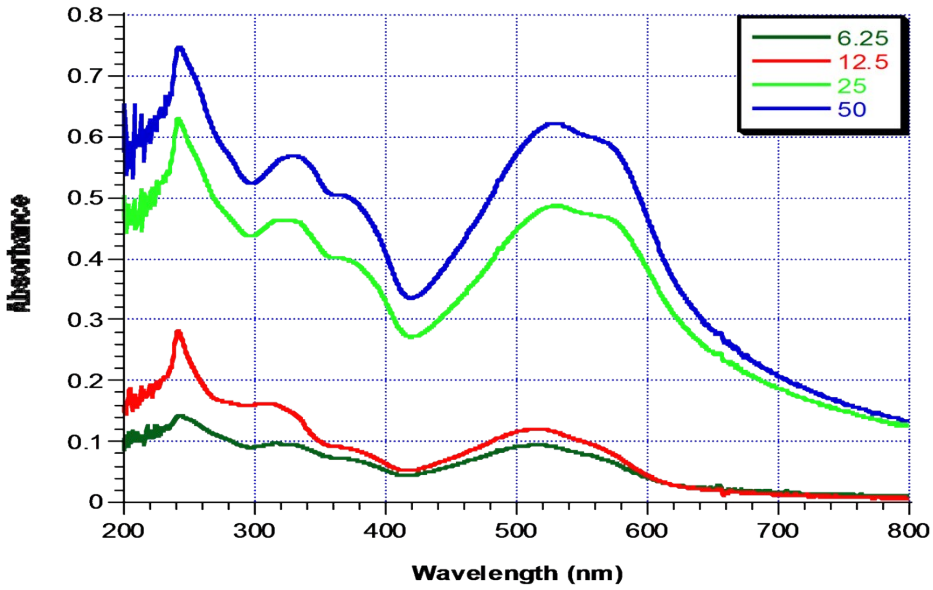

Figure S8. UV spectra of chloroform solution of the host-guest systems of multiarm star copolymers containing PG_{2400} core

Figure S8 shows the arm number of multiarm star copolymers containing PG_{2400} core. As it can be seen, difference between absorption of multiarm star copolymers synthesized by [LA]/[OH] = 25 and 50 ratios is more than that between other ratios.

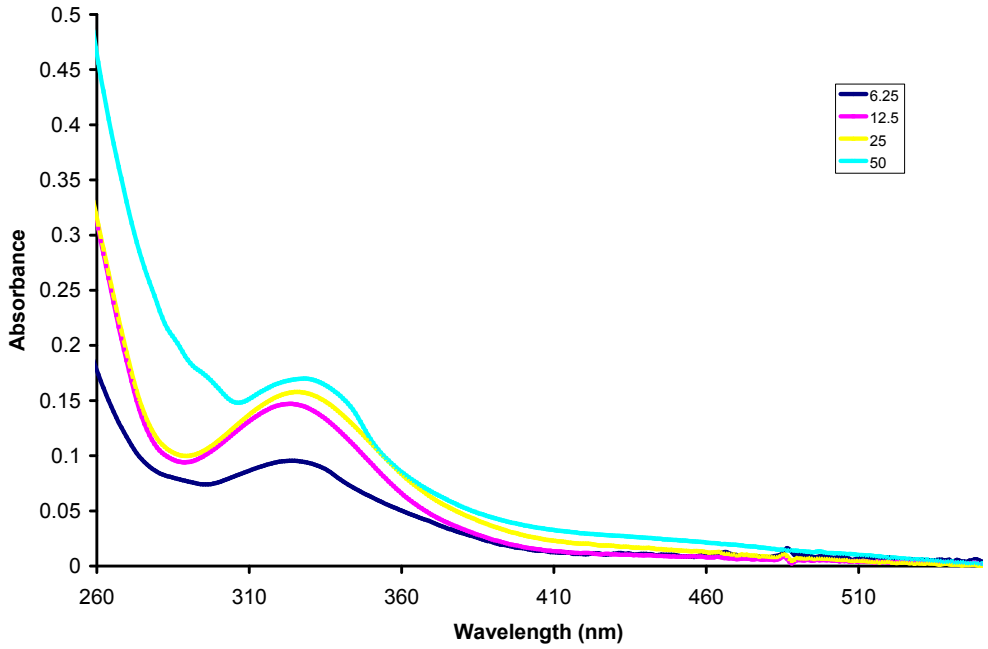

Figure S9. UV spectra of encapsulated 5-ASA by multiarm star copolymers containing hPG_{2400} core and synthesized by 6.25, 12.5, 25 and 50 [LA]/[OH] ratios in chloroform solution

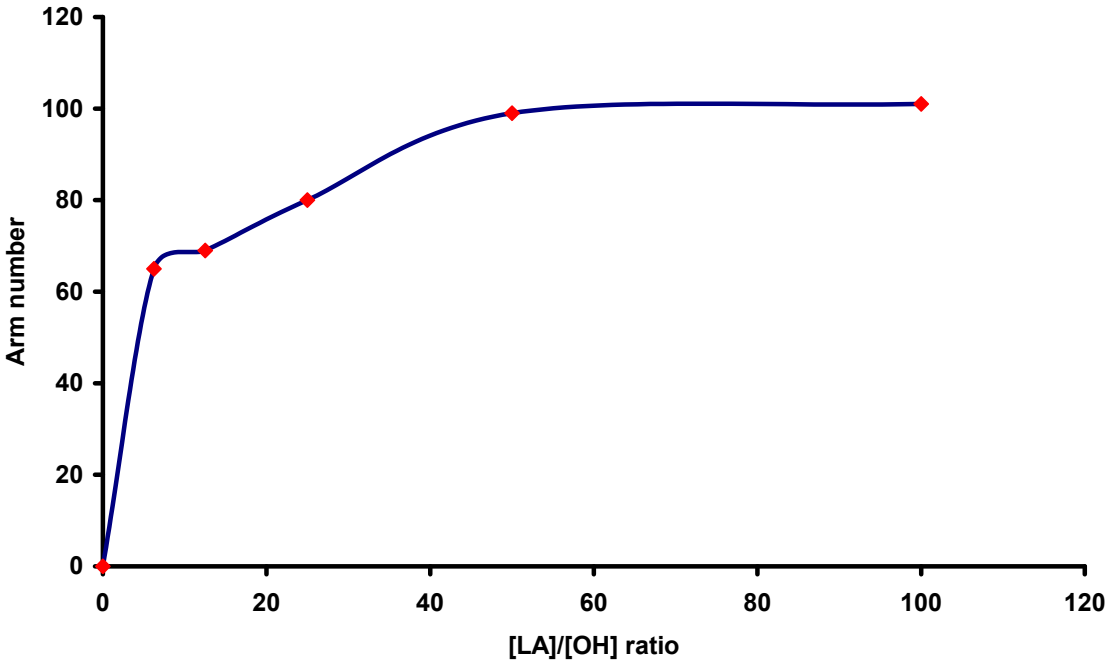

Figure S10. Arm number versus the [LA]/[OH] ratio for multiarm star copolymers containing PG_{8000} core

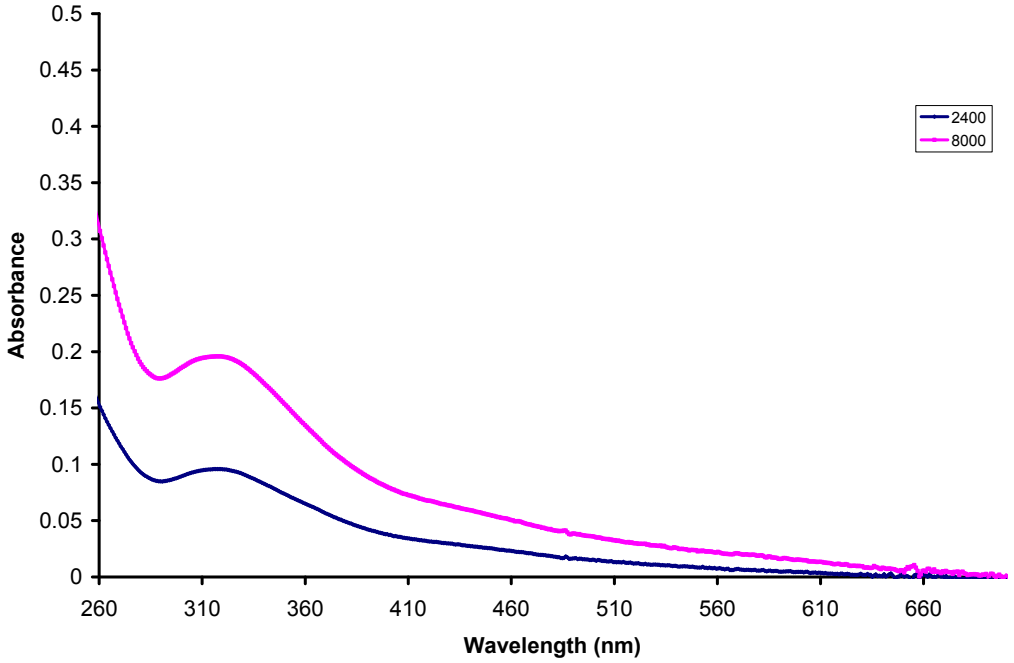

Figure S11. UV spectra of encapsulated 5-ASA by PG_{8000}-PC_{25} and PG_{2400}-PC_{25} multi arm star copolymers

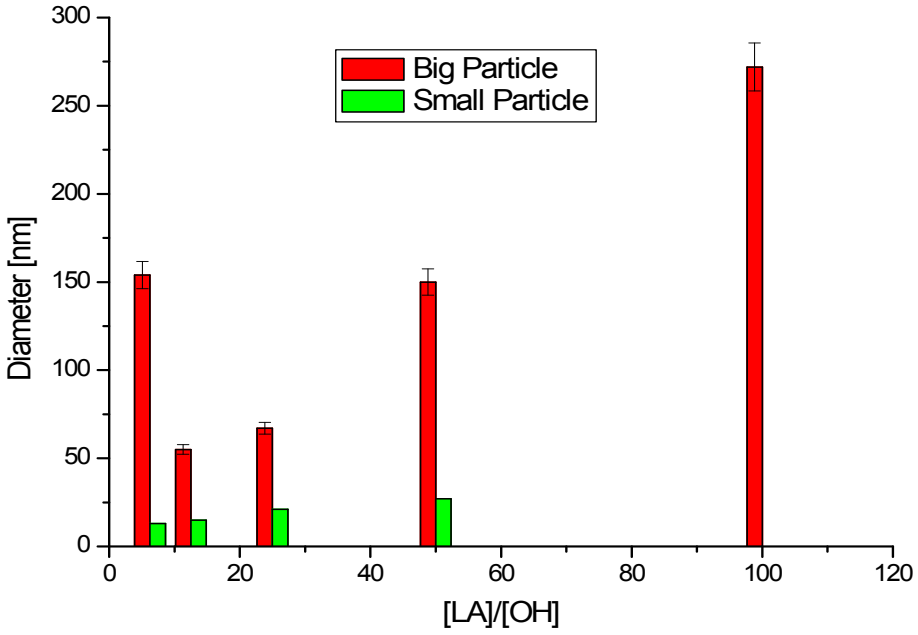

Figure S12. Size of nanocarriers constructed using different ratio of [LA]/[OH] and PG_{8000} core in chloroform.

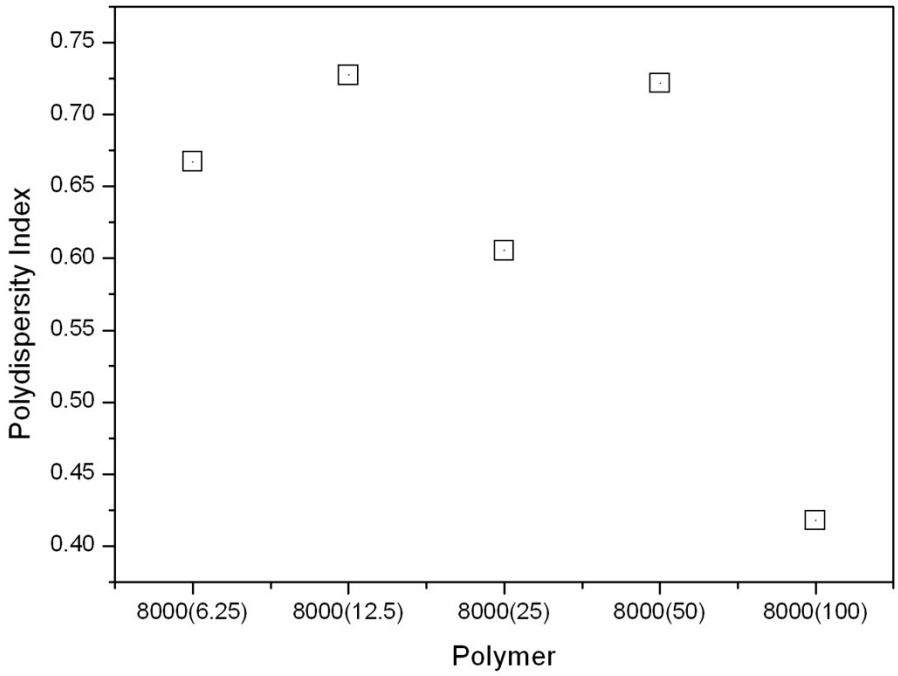

Figure S13. Polydispersity of nanocarriers constructed using different ratio of [LA]/[OH] and PG_{8000} core in chloroform solvent

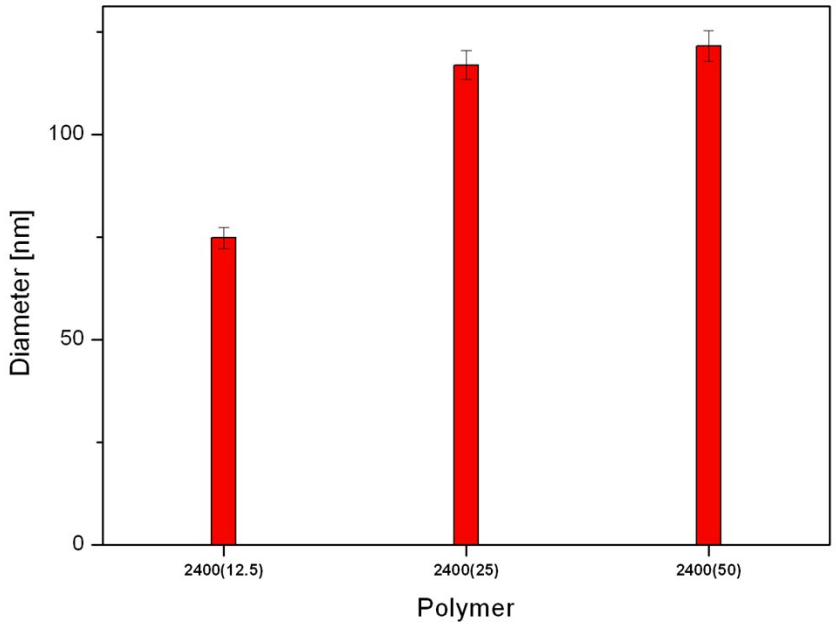

Figure S14. Size of nanocarriers constructed using different ratio of [LA]/[OH] and PG_{2400} core

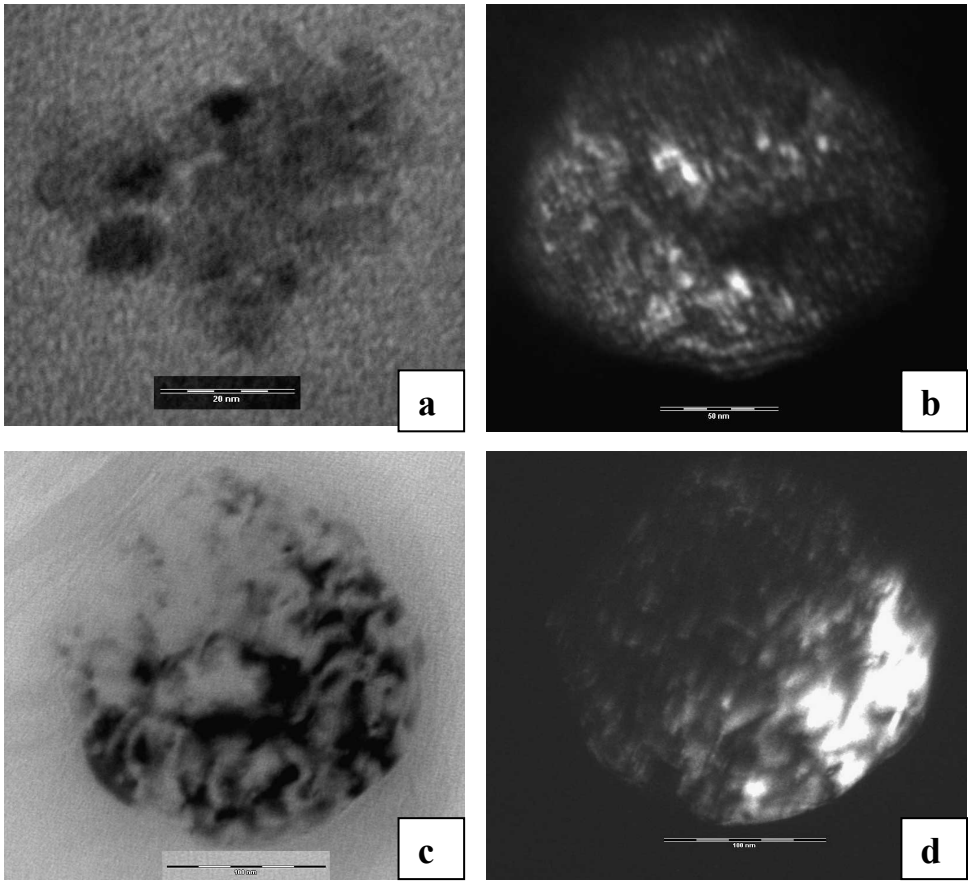

Figure S15. TEM of solid nanocarriers obtained by evaporation of chloroform from a) 0.4 g/L, b) 1 g/L, c and d) 5 g/L solution of nanocarriers

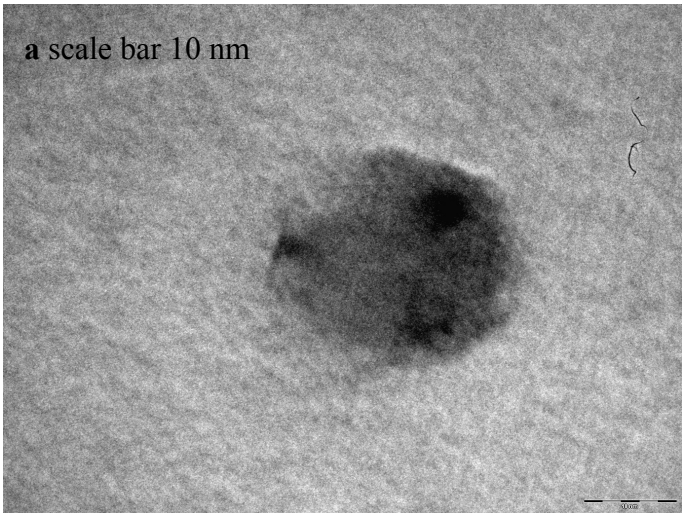

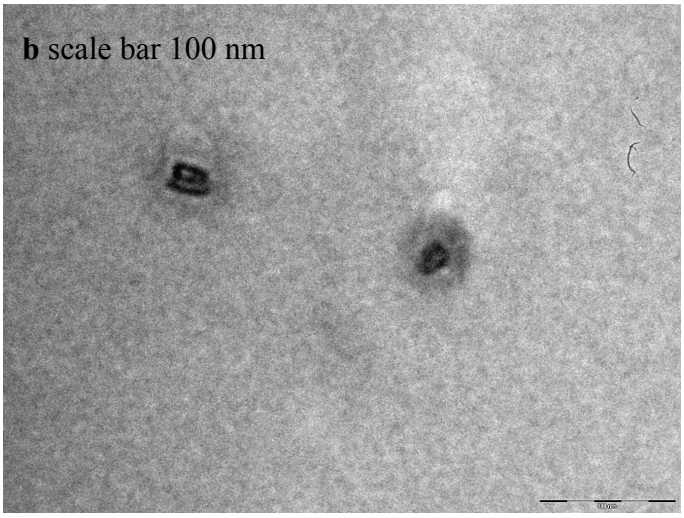

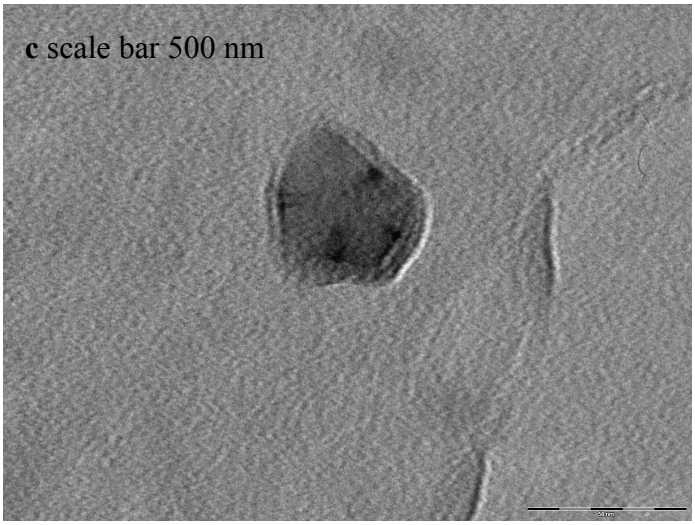

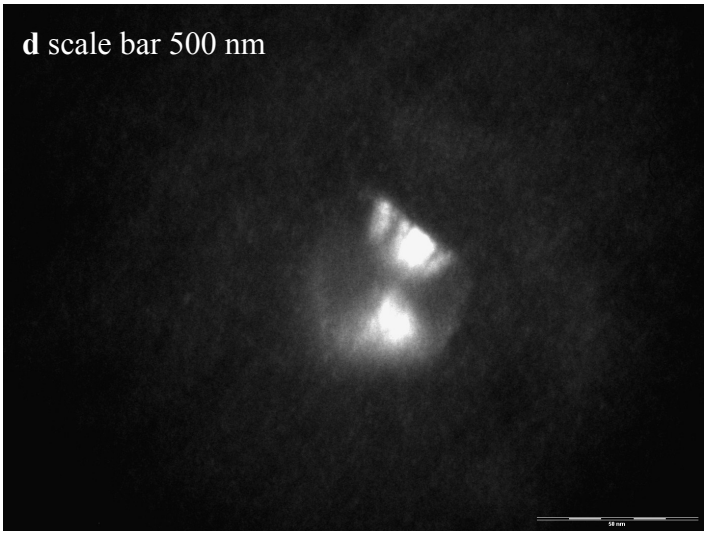

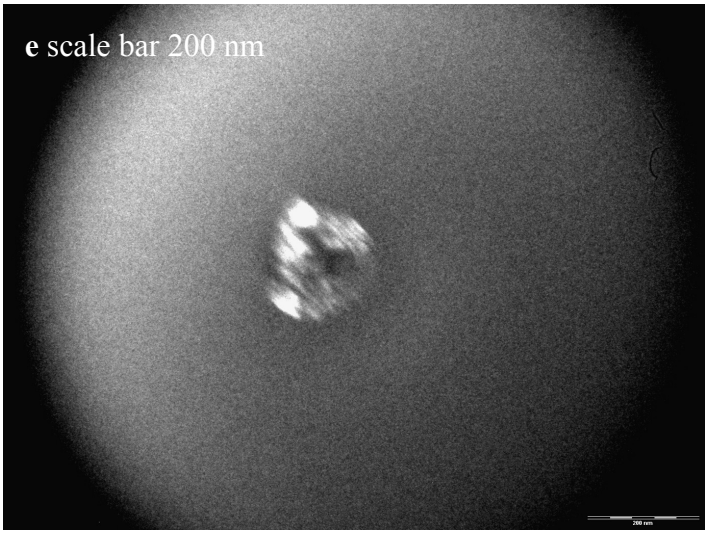

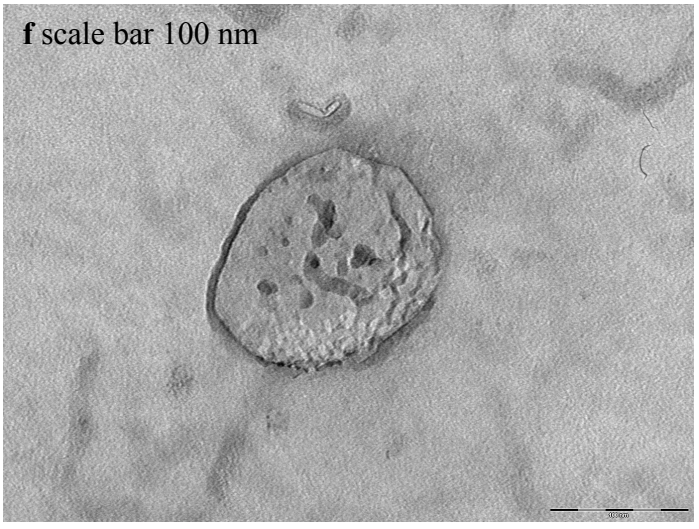

Figure S16. TEM of solid nanocarriers obtained by evaporation of chloroform from a, b, c and d) 0.4 g/L, e) 1 g/L and f) 5 g/L solution of nanocarriers

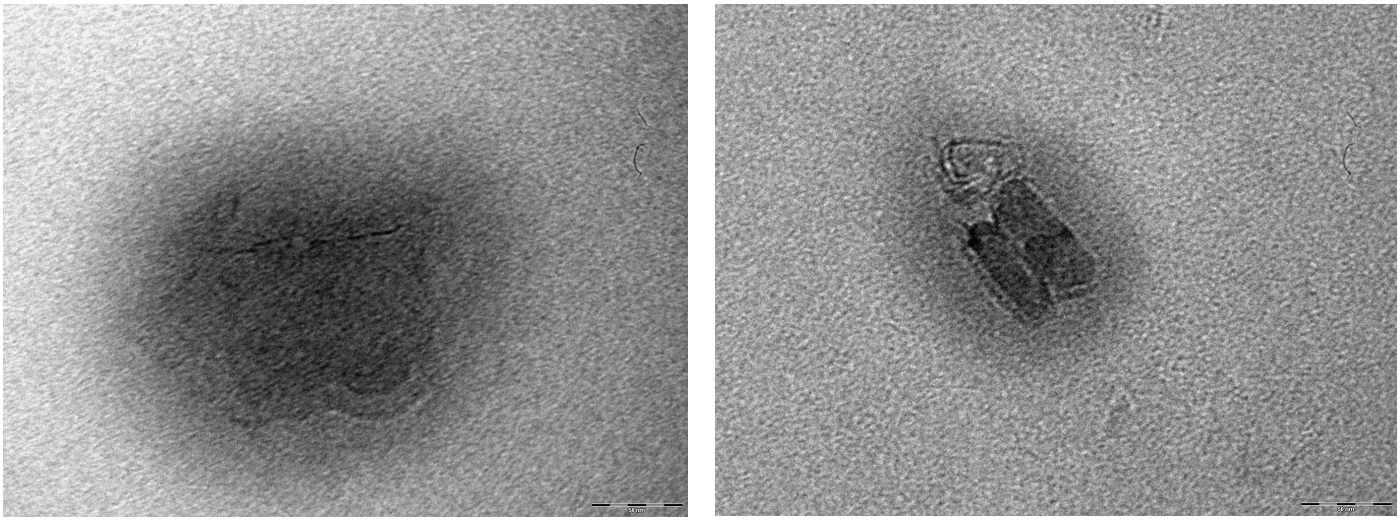

Figure S17. TEM images of solid hPG_{8000}-PLA_{25} nanocarriers, Scale bar is 50 nm.

In order to investigate of the release of guest molecules, water was added to the chloroform solutions of these host-guest systems and mixture was kept at room temperature. The release of the encapsulated guest molecules from chloroform phase to water was investigated by UV-Vis (Figures S18 and S19 (Ø= 20mm). The release rate and amount of released guest molecules from the nanocarrier depends on factors such as arm number and length of arms. In both cases (except 150 for PG_{8000}), the amount of released drug with increasing molecular weight also increases, which is not surprising because the amount of guest molecules carried by the host rises with the molecular weight. In both series, there was a direct relationship between times of maximum release

and molecular weight of star copolymers. The release rate of guest molecules from PG_{2400}-PLA nanocarriers was much higher than for the PG_{8000}-PLA, since PG_{2400}-PLA copolymers are containing a lower number of arms but longer than their analogs' with PG_{8000} core. Therefore, the number of arms seems a more effective factor than the length of arms in regard to the release rate of guest molecules from host molecules as it was also observed for the TC.

Diffusion of Polymers

Evaluation the release of the guest molecules from nanocarriers show that concentration of the free guest molecules increase against the time but after a certain time (depends on star copolymer) concentration of released (free) guest molecules in solution decreases. Hence an experimental work on the PG_{8000}-PLA_{25} and PG_{8000}-PLA_{100} candidates was carried out to examine the diffusion of amphiphilic copolymers to the aqueous phase and re-encapsulation of the released guest molecules supposition. Therefore, solutions of Congo red in water and amphiphilic copolymers in chloroform (with exact molar concentration) were mixed. UV experiments on the aqueous phase showed a decrease in intensity of Congo red's λ_{max} against the time which is related to the diffusion of amphiphilic polymers from the chloroform phase to the interface of the two phases and encapsulation of the dye. The concentration of Congo red was calculated using a calibration curve of Congo red. Results are shown in Figures S20 and S21 for PG_{8000}-PLA_{25} and PG_{8000}-PLA_{100}, respectively. Hence decreasing of the concentration of released guest molecules may be due to the encapsulation of free Congo red through diffusion of star copolymers to the interface of water and chloroform. After 72 h the total decreasing in the concentration of Congo red in water phase for PG_{8000}-$PLA_{12.5}$ and PG_{8000}-PLA_{100} was 0.05 Mol/Lit and 0.14 Mol/Lit respectively. Therefore the total encapsulated Congo red after 72 h by PG_{8000}-PLA_{100} was higher than for PG_{8000}-$PLA_{12.5}$, because the transport capacity of PG_{8000}-PLA_{100} is much higher than for PG_{8000}-$PLA_{12.5}$.

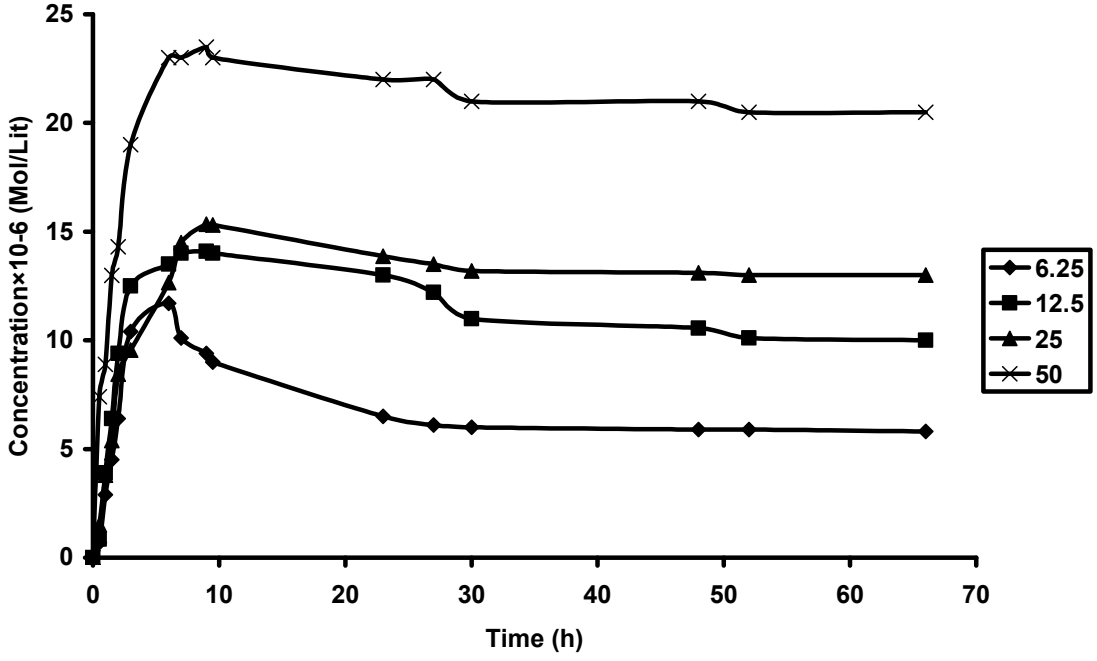

Figure S18. Release of guest molecule from chloroform solution of PG_{2400}-PLA nanocarriers to the water phase.

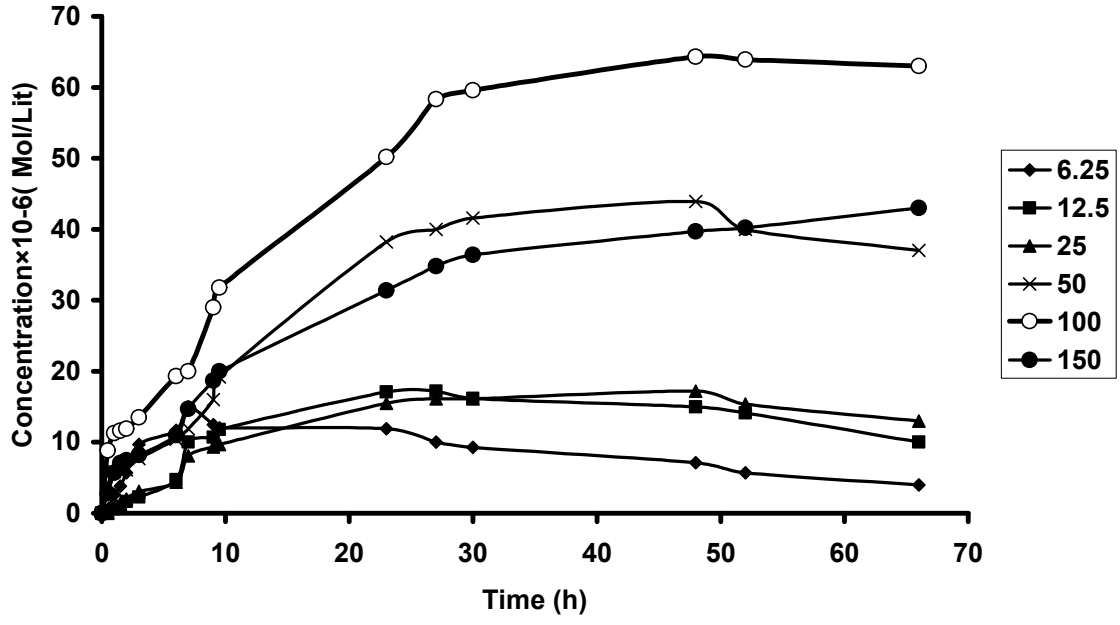

Figure S19. Release of guest molecule from chloroform solution of PG_{8000}-PLA nanocarriers to the water phase.

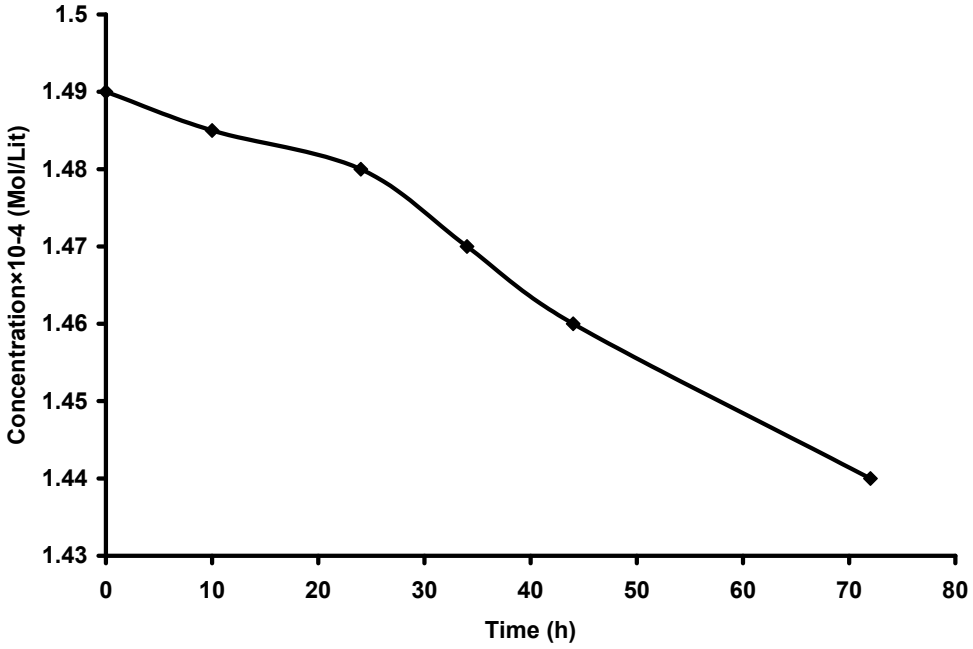

Figure S20. Encapsulation of Congo red by PG_{8000}-PLA_{25} nanocarrier.

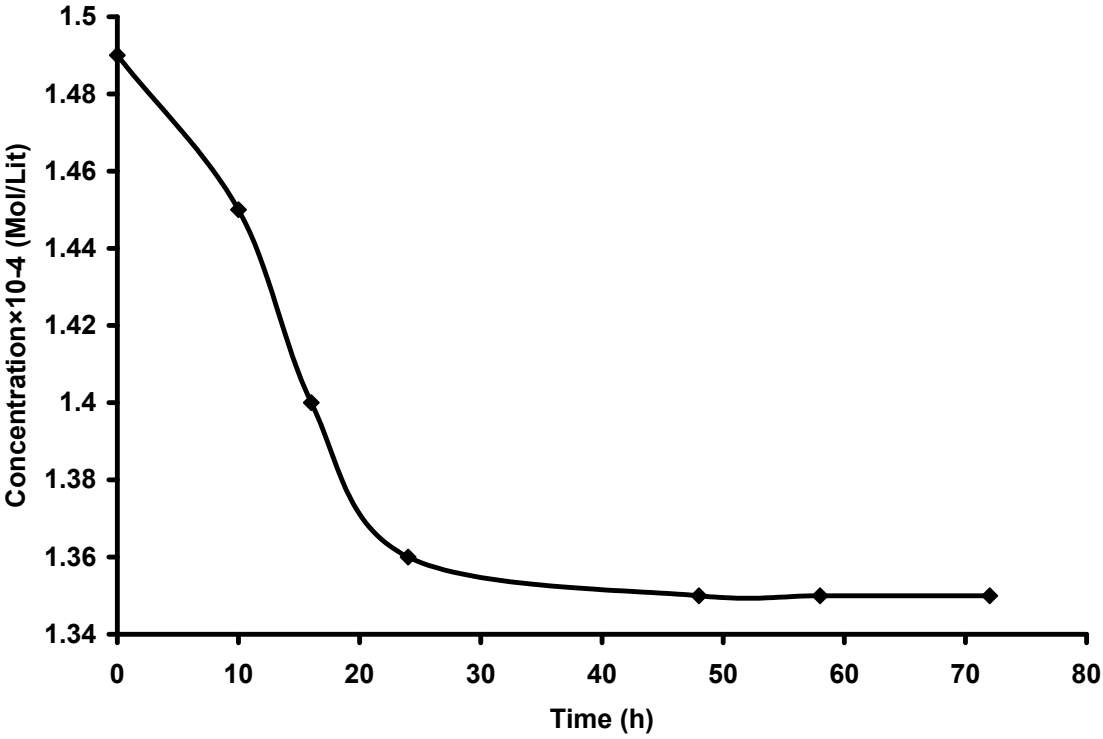

Figure S21. Encapsulation of Congo red by PG_{8000}-PLA_{100} nanocarrier.

Figures S22a and b show the release of 5-ASA from host-guest systems containing PG_{8000}-PLA and PG_{2400}-PLA nanocarriers respectively, at pH 1. It seems here the rate of release of drug is faster than release of drug from conjugated systems, this is logical because here interactions between drug and nanocarriers are only noncovalent type. In this pH after 100 minutes 40-50% of delivered drug is released but after this fast release the rate of release is slow and release of drug from these systems is continued more than three days.

Rate of release of drug from PG_{8000}-PLA nanocarriers is relatively lower than PG_{2400}-PLA nanocarriers (figure S22b). This is related to the structure of multiarm star copolymers.

Figures S23a and b display the release of 5-ASA from host-guest systems containing PLA arms and dendritic PG_{2400} and PG_{8000} cores at pH 7.4.

Here the rate of release is slower than pH 1, on the other hand again rate of release of drug from nanocarriers containing PG_{2400} core is much more than their analogs containing PG_{8000} core.

Figures S24a and b display release of 5-ASA from PG_{2400}-PLA and PG_{8000}-PLA nanocarriers at pH 12 respectively. The rate of release is much higher than other pHs and after 1 h most of drug is released. This behavior is logical, because deprotonation of acidic and phenolic groups of 5-ASA in the basic medium increase its hydrophilicity. On the other hand rate of release of drug from PG_{8000}-PLA is relatively more than PG_{2400}-PLA , this behavior is opposite the behavior of these nanocarriers in the other pHs and may be it is related to the stronger interaction between PG_{8000} and basic buffer, because its free hydroxyl groups is more than PG_{2400}.

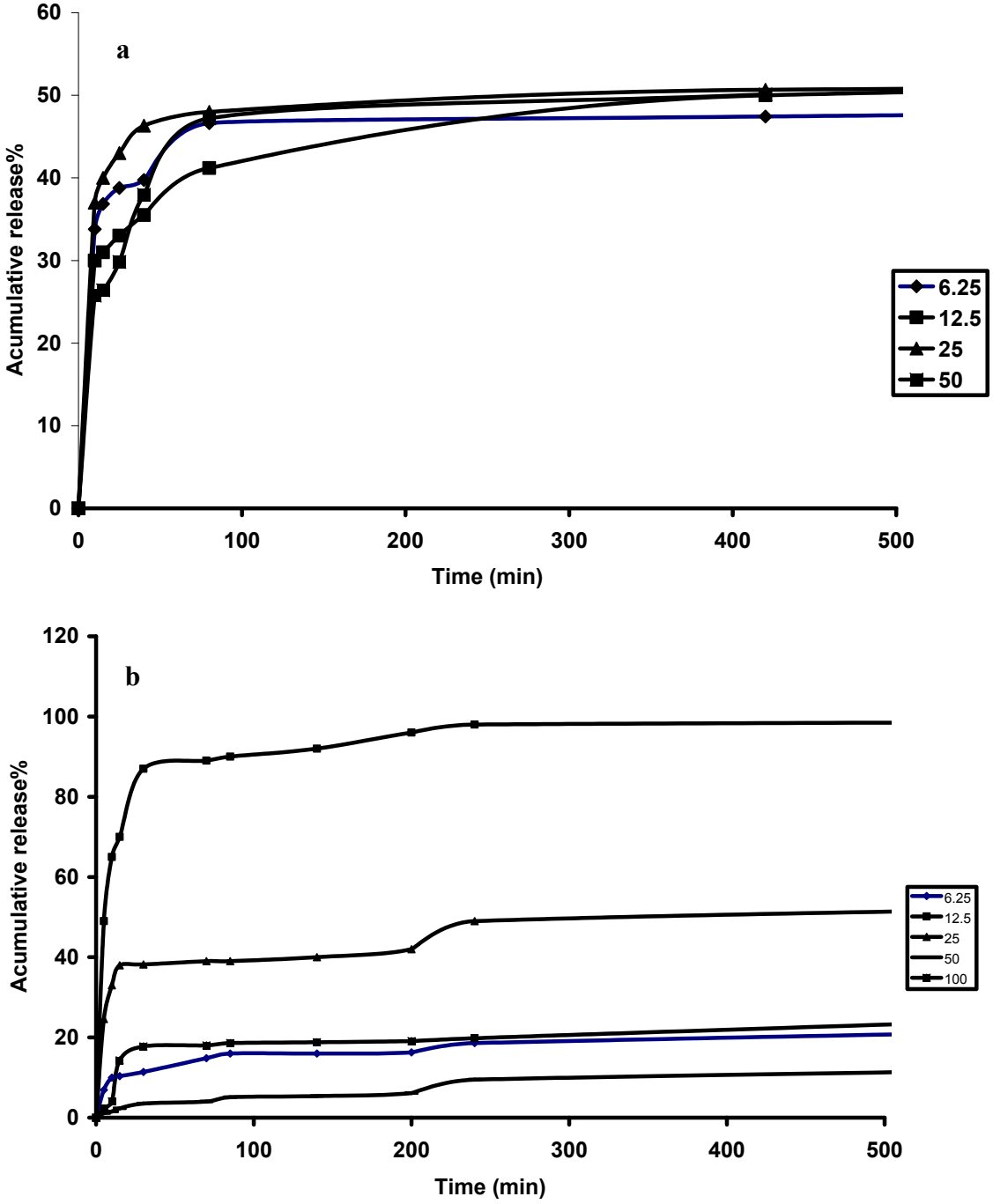

Figure S22. Release of 5-ASA from host-guest systems containing a) PG_{8000}-PLA and b) PG_{2400}-PLA nanocarriers at pH 1.

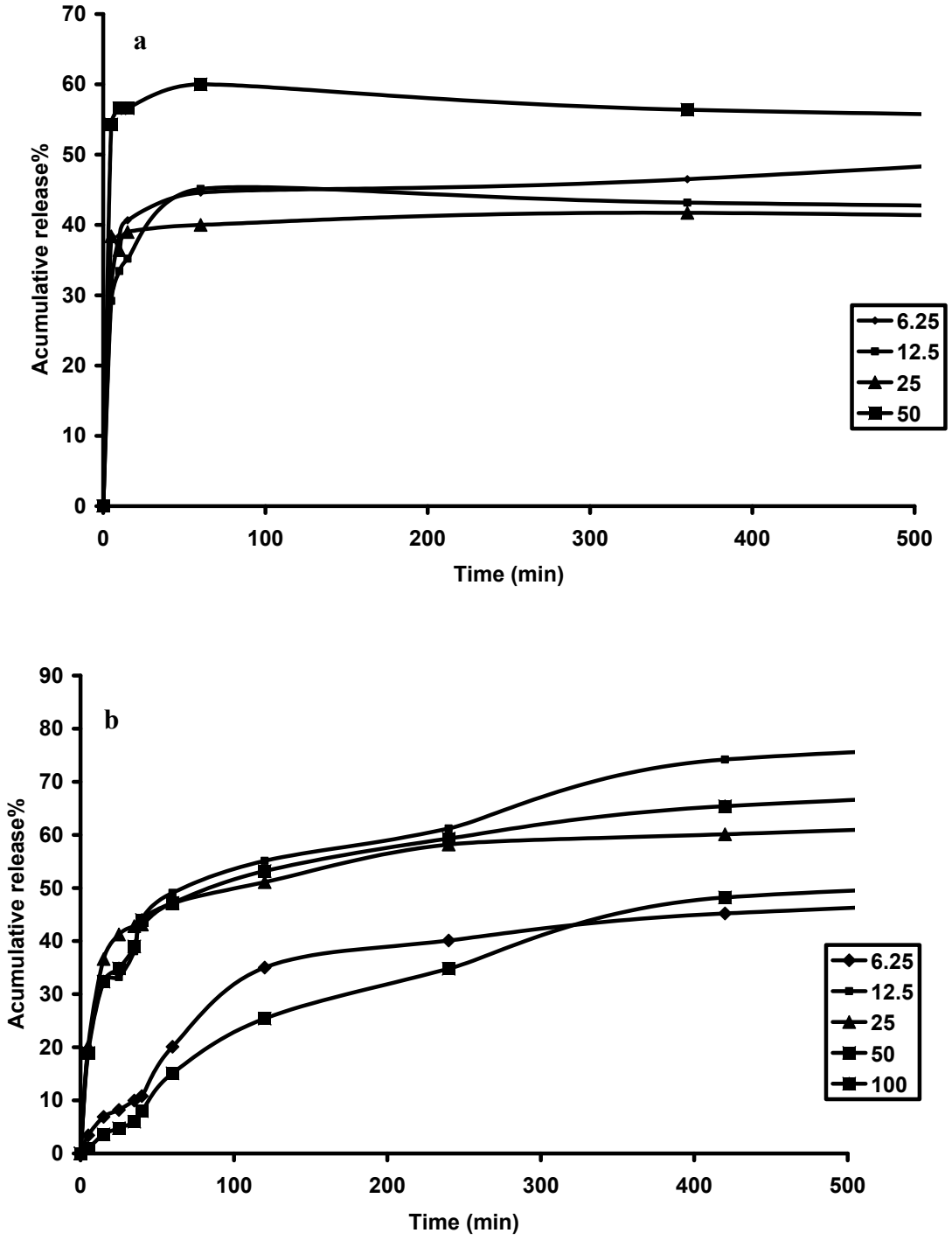

Figure S23: Release of 5-ASA from host-guest systems containing a) PG_{2400}-PLA b) PG_{8000}-PLA at pH 7.4.

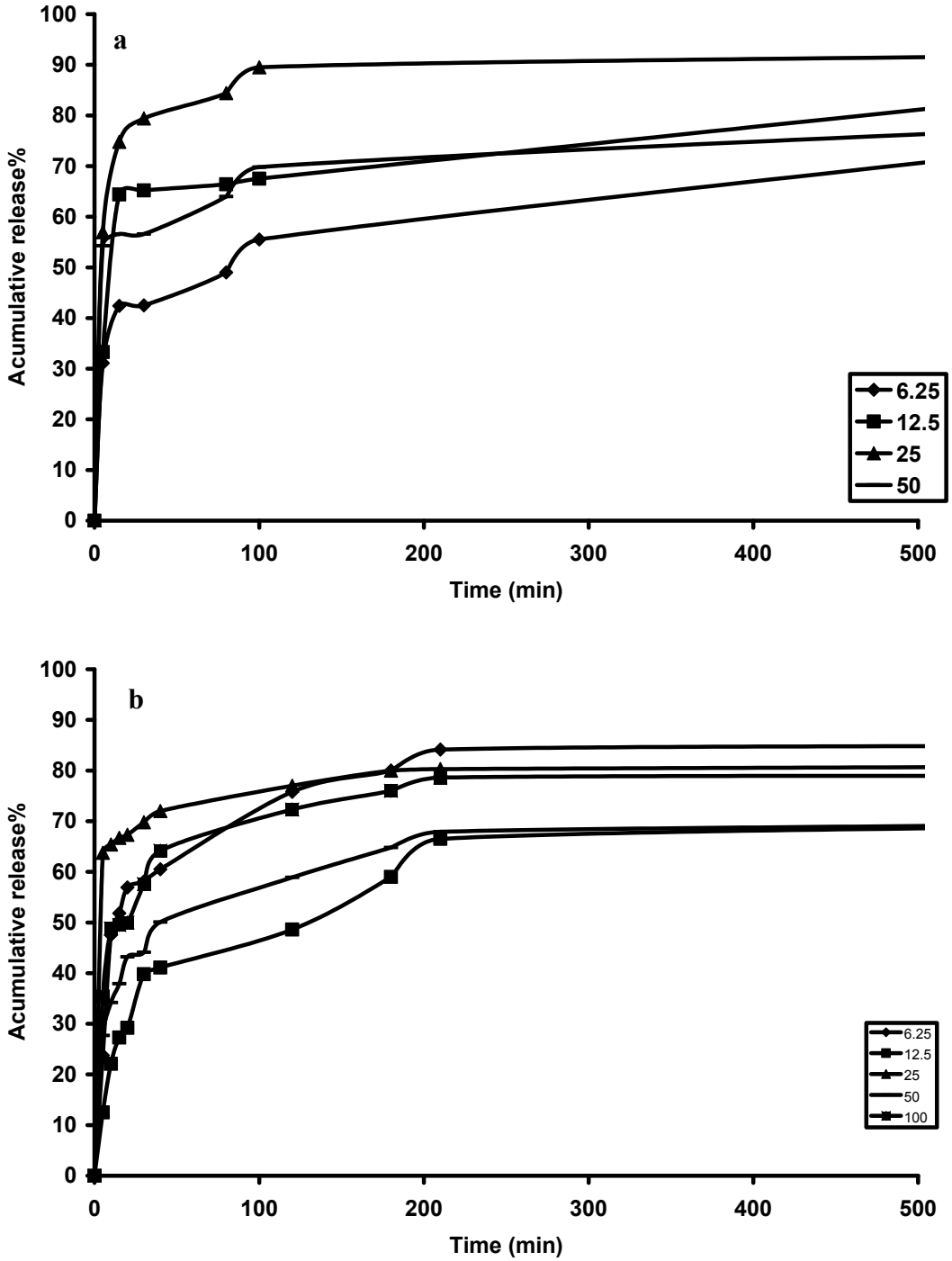

Figure S24: Release of 5-ASA from a) PG_{2400}-PLA and b) PG_{8000}-PLA nanocarriers at pH 12.

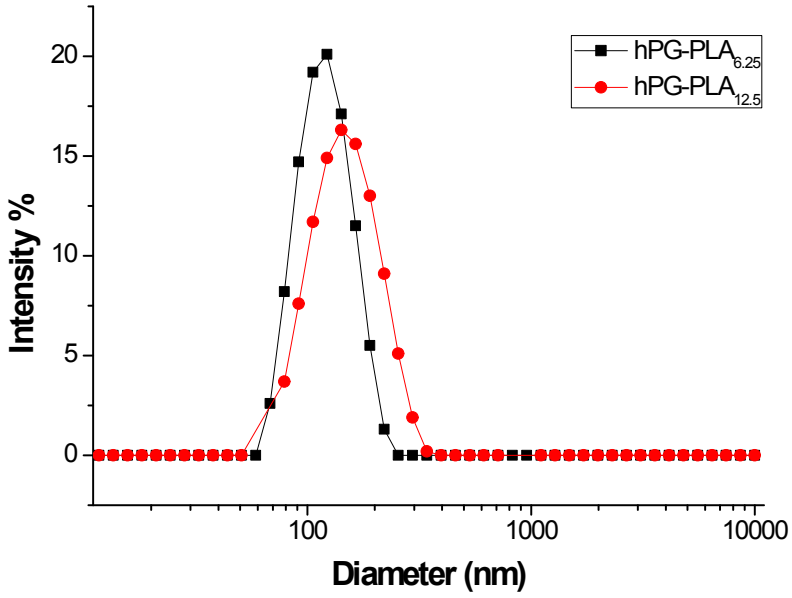

Figure S25: DLS diagrams of PG_{8000}-$PLA_{6.25}$ and PG_{8000}-$PLA_{12.5}$ nanocarriers in water at polymer concentration of 0.5 mg/ml.

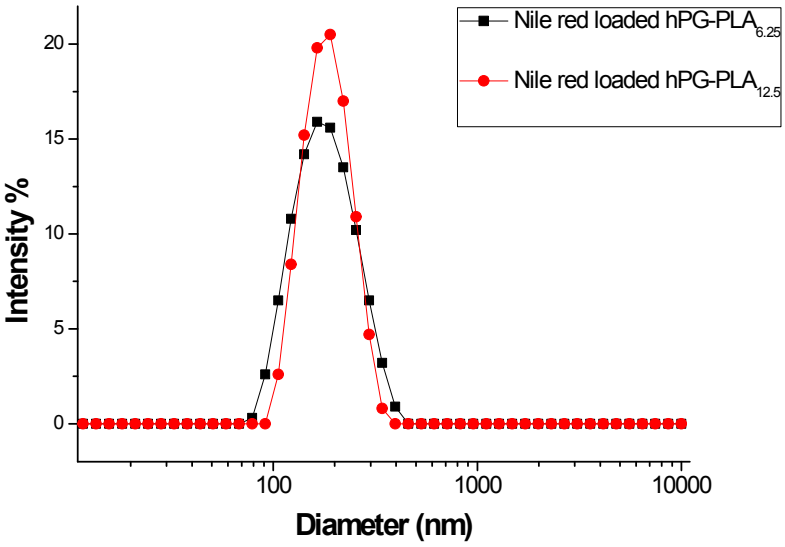

Figure S26: DLS diagrams of PG_{8000}-$PLA_{6.25}$ and PG_{8000}-$PLA_{12.5}$ nanocarriers containing Nile red in water at polymer concentration of 0.5 mg/ml.

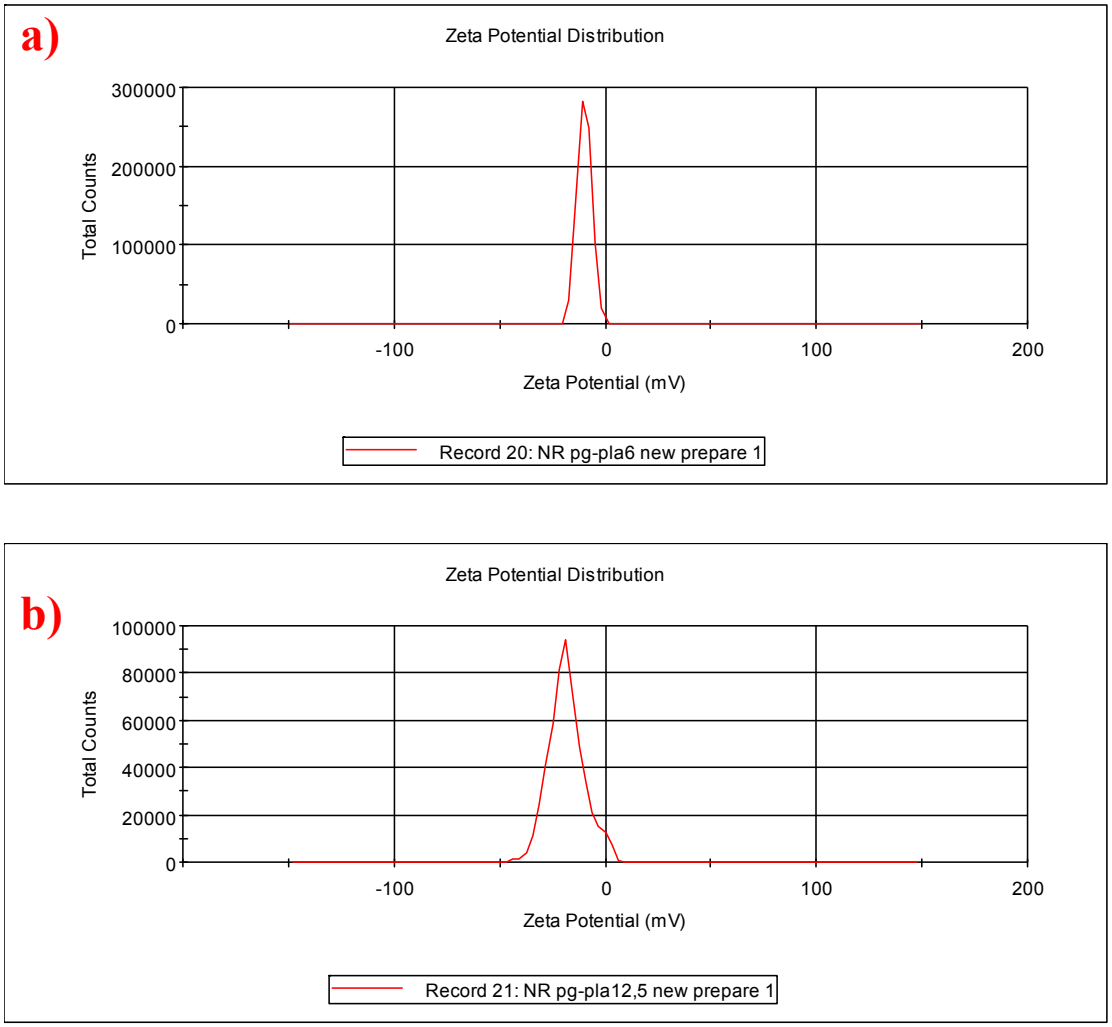

Figure S27: Zeta-potential diagrams of a) PG_{8000}-$PLA_{6.25}$ and b) PG_{8000}-$PLA_{12.5}$ nanocarriers containing Nile red in water at polymer concentration of 0.5 mg/ml.

At pH 7, the PG_{8000}-$PLA_{6.25}$ and PG_{8000}-$PLA_{12.5}$ without loading and after loading Nile red have a large negative zeta potential. This may be attributed to the presence of ionised carboxyl groups on the nanosphere surface [1, 2].

The figure S25 and S26 showed the diameters of PG_{8000}-$PLA_{6.25}$ and PG_{8000}-$PLA_{12.5}$ without loading and after loading Nile red. The neat nanocarriers have an average size as 116.1±0.95 (PDI 0.059) and 134.7±5.01 (PDI: 0.083) for PG_{8000}-$PLA_{6.25}$ andPG_{8000}-$PLA_{12.5}$ respectively. After loading Nile red, both two display increased size, determined as 169.1 ±0.95（PDI 0.091）and 176.4±1.15 (PDI: 0.058), respectively. PG_{8000}-

$PLA_{12.5}$ due to its longer PLA chain, result to a larger particle size is quite reasonable. Besides, figure S27 showed the zeta potential of Nile red loaded PG_{8000}-$PLA_{6.25}$ andPG_{8000}-$PLA_{12.5}$ are -28.6mV and -27.5mV.

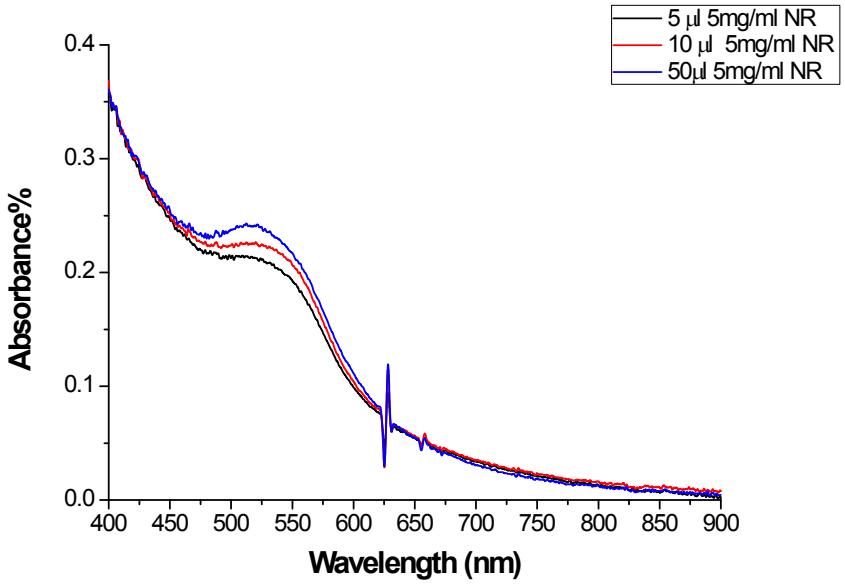

Figure S28: UV spectra of encapsulated Nile red by PG_{8000}-$PLA_{12.5}$ nanocarriers in water with 0.5mg/ml polymer concentration and increased Nile red amount.

1. S. Stolnik, M.C. Garnett, M.C. Davies, L. Illum, M. Bousta, M. Vert, S.S. Davis, Colloids Surf. A: Physicochem. Eng. Aspects 1995, **97**, 235.
2. D. Chognot, J.L. Six, M. Leonard, F. Bonneaux, C. Vigneron, E. Dellacherie. Journal of Colloid and Interface Science 2003, **268**, 441.